



## Sediment inception under breaking tidal bores

Nazanin Khezri, Hubert Chanson\*

The University of Queensland, School of Civil Engineering, Brisbane QLD 4072, Australia

### ARTICLE INFO

#### Article history:

Received 21 September 2011  
Received in revised form 31 January 2012  
Available online 5 March 2012

#### Keywords:

Geophysical flows  
Sediment transport inception  
Physical modelling  
Tidal bores  
Bed load  
Longitudinal pressure gradient

### ABSTRACT

A tidal bore may develop in an estuary during the spring tide conditions when the tidal range exceeds 5–6 m and the flood tide is confined to a narrow funnelled estuary with low freshwater levels. The tidal bore is of great importance for the geomorphology of the estuarine zone. In this study, some physical modelling was performed to investigate the sediment motion inception beneath a tidal bore on a movable gravel bed. The results show the significant impact of breaking bore propagation on the gravel bed motion. The dominant contribution to sediment transport inception is the longitudinal pressure gradient force, while the transient recirculation motion next to the bed yields to a drag force acting in the upstream direction and contributing to sediment motion.

© 2012 Elsevier Ltd. All rights reserved.

### 1. Presentation

A tidal bore is a series of waves propagating upstream as the tidal flow turns to rising. It forms during the spring tides when the tidal range exceeds 5–6 m and the flood tide is confined to a narrow funnelled estuary with low freshwater levels. The shape of the tidal bore is directly linked with its Froude number  $Fr = (V_0 + U)/\sqrt{g \times d_0}$  where  $V_0$  and  $d_0$  are the initial flow velocity and depth,  $g$  is the gravity acceleration and  $U$  is the tidal bore celerity. Some famous tidal bores are those of Qiantang River (China), Amazon River (Brazil) and Seine River (France). When a tidal bore forms in a narrow funnelled channel, its upstream propagation induces some intense turbulent mixing resulting in bed erosion and upstream sediment advection (Chen et al., 1990; Tessier and Terwindt, 1994; Koch and Chanson, 2009; Lubin et al., 2010). However no study investigated to date the sediment motion beneath a tidal bore under controlled flow conditions.

In this study, the turbulent mixing of tidal bores is investigated physically with a focus on sediment transport inception. A physical study based upon a Froude dynamic similarity is presented with experiments performed on a movable gravel bed. The results in terms of sediment particle tracking shows the leading role of the longitudinal pressure gradient beneath the tidal bore in destabilising the particles while the drag force and virtual mass force maintain the upstream sediment flux.

### 2. Theoretical considerations

In a non-uniform open channel flow, the parameters relevant to sediment motion inception for non-cohesive materials include the shear stress  $\tau$  of the fluid on the particle, the fluid density  $\rho$ , the fluid viscosity, the sediment relative density  $S$ , the particle size  $d_s$  and shape, the gravity acceleration  $g$  and bed slope  $\theta$ , as well as the longitudinal pressure gradient term  $\partial P/\partial x$  and water depth  $d$  (Julien, 1995; Chanson, 1999):

$$F_1 \left( \tau, d, \rho, \mu, S, d_s, \text{shape}, g, \theta, \frac{\partial P}{\partial x} \right) = 0 \quad (1)$$

In dimensionless terms it yields:

$$F_2 \left( \frac{\tau}{\rho \times (S-1) \times g \times d_s}, S, \frac{d_s}{d}, \frac{d_s \times \sqrt{\rho \times \tau}}{\mu}, \text{shape}, \frac{\partial P/\partial x}{\rho \times g \times (S-1)} \right) = 0 \quad (2)$$

In presence of a movable bed, the forces acting on a sediment particle include the gravity force, the buoyancy force, the shear/drag force, the lift force, the resultant of the reaction forces of the surrounding grains, the longitudinal pressure gradient, the Magnus force, the virtual mass force and the Basset history force. Note that the gravity and buoyancy forces act along the vertical direction, while the lift force acts in the direction perpendicular to the flow and the shear force acts along the flow direction (Fig. 1). The virtual mass force is imposed on the particle in a fluid due to the fluid or body acceleration, and it acts on the surfaces in contact with the fluid (Brennen, 1982). The Basset history force is a history

\* Corresponding author. Tel.: +61 7 3365 3516; fax: +61 7 3365 4599.  
E-mail address: [h.chanson@uq.edu.au](mailto:h.chanson@uq.edu.au) (H. Chanson).

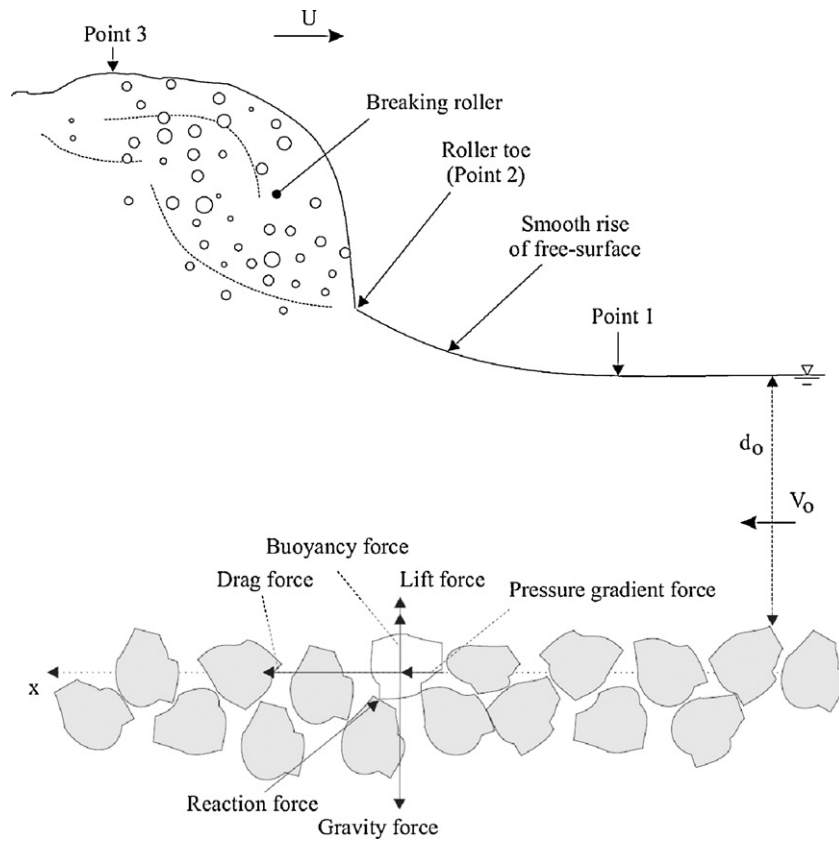


Fig. 1. Sketch of a breaking tidal bore propagating upstream and incomplete force diagram on non-cohesive sediment particles—not all forces shown for clarity.

term which indicates that the resistance to motion at a given time is in part a function of the resistance at a previous time (Nino and Garcia, 1998).

Considering a fully submerged sediment particle initially at rest on a horizontal channel bed, the forces acting on a particle initially at rest include the shear/drag force, a pressure force, a virtual mass force, the resultant of intergranular forces, the weight force. In first approximation, the equation of motion for the particle in the longitudinal  $x$ -direction may be simplified into:

$$m_s \times \frac{\partial V_s}{\partial t} \cong F_{shear} + F_p + F_{virtual} \quad \text{in the longitudinal } x\text{-direction} \quad (3)$$

The shear/drag force equals:

$$F_{shear} = \frac{1}{2} \times C_d \times \rho \times (V - V_s) \times |V - V_s| \times A_s \quad (4)$$

where  $A_s$  is the area of the sediment particle in the  $x$ -direction,  $\rho$  is the water density,  $V$  is the fluid velocity positive downstream,  $|V|$  is the velocity magnitude,  $C_d$  is a drag coefficient encompassing surface shear and form drag and  $V_s$  is the particle velocity positive in the same direction as the fluid velocity.

In presence of a longitudinal pressure gradient  $\partial P/\partial x$ , the pressure gradient force for a fixed particle equals:

$$F_p = -\frac{\partial P}{\partial x} \times A_s \times h_s \quad (5)$$

where the minus sign reflects that a positive pressure gradient induces a negative force and  $h_s$  is a characteristic particle size. For a spherical particle (diameter  $d_s$ ) and assuming a constant pressure gradient across the particle, it becomes:

$$F_p = -\frac{\partial P}{\partial x} \times \frac{\pi \times d_s^3}{6} \quad (6)$$

Note the approximation of a constant longitudinal pressure gradient  $\partial P/\partial x$  which might not be appropriate for large size particles next to the roller toe, since  $\partial P/\partial x$  might tend to an infinite value there (Fig. 1, Point 2).

The virtual mass force equals:

$$F_{virtual} = m_f \times C_m \times \frac{\partial(V - V_s)}{\partial t} \quad (7)$$

where  $m_f$  is the mass of displaced fluid ( $m_f = m_s/S$ ), and  $C_m$  is an added mass coefficient. The virtual mass coefficient is a function of the particle shape and flow conditions (Brennen, 1982).

Herein Eq. (3) is tested against physical measurements under controlled flow conditions.

### 3. Physical study

#### 3.1. Presentation

The experiments were performed in a 12 m long 0.5 m wide rectangular channel equipped with glass walls. The bed was made of a series of plywood sheets covered by blue granite gravels ( $S=2.65$ ) sieved between 4.75 and 6.70 mm. The gravel material was glued in resin but for a 1 m long section (located between  $x=4.5$  and 5.5 m) with a layer of identical but loose gravels spread evenly before each experiment. The mobile bed was about 2–3 grain size thick. The water was supplied by a constant head tank. A fast-closing tainter gate was located at  $x=11.15$  m where  $x$  is the longitudinal distance from the channel upstream end and the gate was closed rapidly to generate a tidal bore propagating upstream in the channel.

The steady water discharge was measured with two orifice meters designed based upon the British Standards. In steady flows, the water depths were measured using rail mounted pointer gauges. The bore propagation was studied with a series of acoustic

**Table 1**  
Experimental flow conditions.

Reference	$Q$ (m <sup>3</sup> /s)	$B$ (m)	$d_o$ (m)	$U$ (m/s)	Fr	Type(s) of bore	Remarks
Present study	0.050–0.052	0.50	0.136	0.6–0.9	1.17–1.4	Undular and breaking	Visual and free-surface observations
	0.051	0.50	0.136	0.87	1.40	Breaking	ADV and particle tracking

Note:  $B$ : rectangular channel width;  $d_o$ : initial flow depth at  $x = 5$  m; Fr: tidal bore Froude number;  $Q$ : initial flow rate;  $U$ : tidal bore celerity at  $x = 5$  m;  $x$ : longitudinal distance from the channel upstream end.

displacement meters Microsonic™ Mic + 25/IU/TC. The turbulent velocity fluctuations were measured at one location ( $x = 5$  m) using an acoustic Doppler velocimeter (ADV) Nortek™ Vectrino equipped with a three-dimensional side-looking head. The particle motion was studied between  $x = 4$  and 6 m with a digital video-camera Panasonic™ NV-GC300 (25 fps). About 20–25 video movies were made and at least 15–20 painted particles were tracked per video. The total number of particles in motion was much larger in each video movie, but only particles within the depth of field of the camera lens were tracked. Further observations were recorded using a SLR camera Pentax™ K-7.

3.2. Flow conditions and tidal bore generation

The setup was chosen to generate an initially steady open channel flow without gravel bed motion. The tidal bore was generated by the rapid closure of the downstream tainter gate; its closure time was less than 0.2 s. After the rapid closure, the bore propagated upstream and each experiment was stopped when the bore front reached the upstream intake structure to avoid any wave reflection.

A first series of experiments was conducted to characterize the flow patterns, free-surface properties and sediment inception conditions (Table 1). A second series of detailed measurements was performed with a breaking bore during which ADV and video data were recorded (Table 1).

4. Results

Some basic observations were conducted with similar initial conditions ( $Q = 0.05$  m<sup>3</sup>/s,  $d_o = 0.136$  m) and a range of Froude numbers Fr (Table 1). Undular bores were observed for the smallest Froude numbers ( $Fr < 1.3$ ). For Froude numbers between 1.2 and 1.3, some slight breaking was observed at the first wave crest next to the channel centreline. At the largest Froude numbers ( $Fr > 1.3$ –1.4), the bore had a marked two-dimensional breaking roller.

For a breaking bore, Fig. 2 presents some typical results in terms of the water elevation above the bed and instantaneous

longitudinal velocity component. Herein  $V_x$  is positive downstream and the characteristic time  $T_2$  corresponds to the passage of the roller toe (as defined in Fig. 1). The propagation of the breaking bore was associated with a rapid rise of the water surface during the breaking roller passage followed by some residual oscillations. The passage of the bore roller corresponded to a strong longitudinal deceleration, associated with a transient recirculation ( $V_x < 0$ ) next to the bed clearly seen between  $t - T_2 = 0.05$  and 2.5 s in Fig. 2.

Prior to the tidal bore, no gravel bed motion was observed. During the undular bores, the sediment movement was negligible. For example, for each video, at most two sediment particles would move briefly, typically as some particle rotation rather than a change in absolute position. With a breaking tidal bore, some significant gravel bed motion was observed during the bore passage. This is illustrated in the video data (Appendix A). In the video movie, the water flowed initially from right to left. The tidal bore propagated from left to right. The passage of the bore induced a sudden gravel bed motion upstream (from left to right). The sediment particle motion was a bed load motion, with an appearance somehow similar to a sudden sheet flow.

The particle motion relative to the tidal bore propagation was compared with three characteristic points of the bore free-surface: (1) the start of the upward free-surface curvature, (2) the toe of the roller and (3) the local maximum in free-surface elevation immediately downstream of the aerated roller (Fig. 1). For the experiment shown in Fig. 2, some typical results in terms of the gravel particle trajectories are presented for a single video record (Fig. 3). In Fig. 3, each particle trajectory is indicated with a letter (A to O), the horizontal axis represents 0.50 m and the co-ordinate  $X$  is positive upstream: that is, a particle motion towards the right side of the video movie.

The upstream particle velocity during the bore passage was on average  $-0.12$  m/s although the maximum particles velocities reached values up to  $-0.60$  m/s. For comparison, the average celerity of the bore was  $U = 0.87$  m/s (Table 1). Note that  $U$  is positive

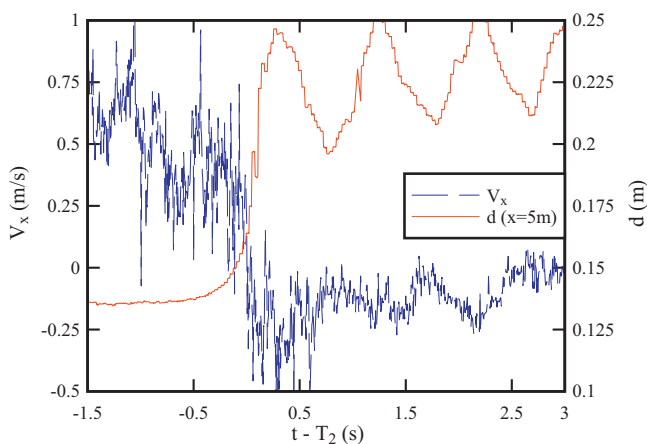


Fig. 2. Instantaneous water depth and longitudinal velocity  $V_x$  measurements in a breaking tidal bore—data: Fr = 1.4,  $x = 5$  m,  $z/d_o = 0.09$ , sampling rate: 200 Hz.

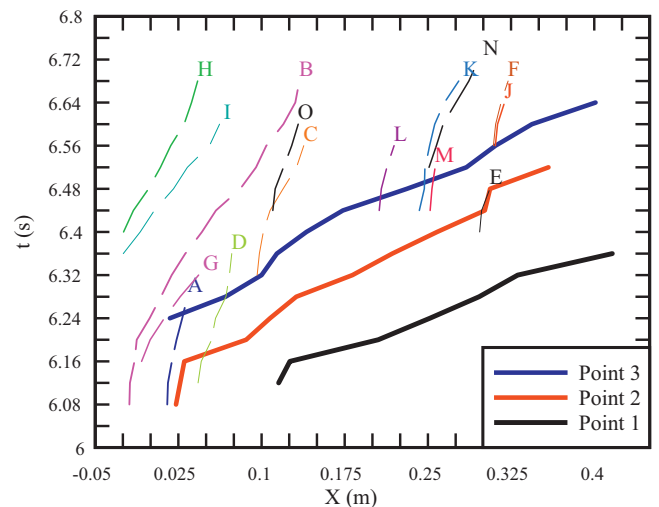
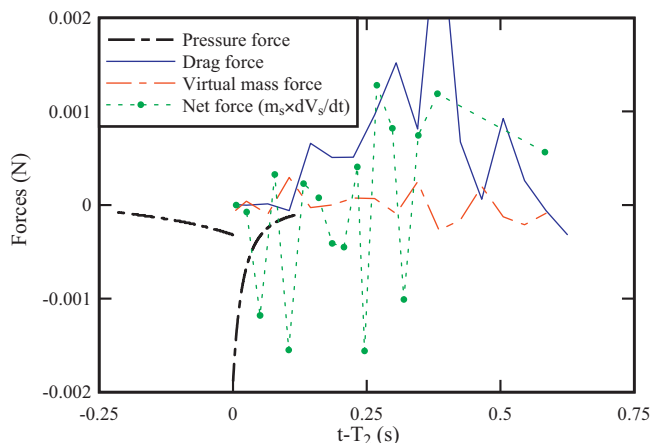


Fig. 3. Gravel particle trajectories as function of time: data: Fr = 1.4, run 32, bed load motion.



**Fig. 4.** Pressure gradient force, drag force and virtual mass force acting on a particle beneath a breaking bore—the net force on the particle is also shown (green filled circles)—data:  $Fr = 1.4$ , run 13. (For interpretation of the references to color in this figure legend, the reader is referred to the web version of the article.)

upstream, while the fluid and particle velocities were positive downstream. The data showed however a range of particle motion. Some particles were advected upstream very rapidly: e.g. particles B, G, I in Fig. 3. The majority of particles were convected at a slower rate. For example, particles A, C, E, F, J, L, M, and O in Fig. 3. The results in terms of duration of particle motion during the bore passage indicated that about 50% of particles moved for longer than 0.3 s. The maximum accelerations of particles were observed at inception and occurred typically immediately after the bore toe ( $t - T_2 \geq 0$ ). Although the maximum particle acceleration was  $4.74 \text{ m/s}^2$  on average, about 10% of particles reach a maximum horizontal acceleration in excess of  $1 \times g$  where  $g$  is the gravity acceleration.

Overall a large number of particles were set into motion by the breaking bore and moved upstream behind the bore. The gravel bed load motion was initiated primarily by the passage of the roller toe (e.g. Fig. 3).

## 5. Discussion

Eq. (3) was tested against the physical measurements. The acceleration term was deduced from the instantaneous particle motion. The longitudinal pressure force was calculated from the free-surface profile. The drag force and virtual force were estimated from the ensemble-averaged longitudinal velocity data. Some typical results for a particle are shown in Fig. 4. The results shown in Fig. 4 suggest that the pressure gradient force had the largest impact on the particle motion inception. The shear force acting on the particle was not the initial driving force of sediment inception. With increasing time, the pressure gradient force decreased, the effect of shear force on the particle motion increased, and the combination of both forces moved the particle upstream for a substantial distance. The particle stopped when the pressure gradient and shear forces no longer acted on the particle. A similar trend was observed for more than 200 particles.

Overall the data analysis showed a number of trends. During the initially steady flow, the drag force on the particle fluctuated around a mean value and was equal to the particle interaction force in absence of particle motion. When the bore passed, the longitudinal pressure gradient force caused by the sudden change in free surface elevation was the predominant force inducing the inception of upstream particle motion. Most particles started to move and reached the highest acceleration when the pressure gradient force was maximum, although some began to move just before or just

after the maximum pressure gradient instant ( $t - T_2 = 0$ ). The shear force magnitude decreased with the sudden deceleration induced by the bore front passage and a negative shear force took place during the transient recirculation (see in Fig. 2 for  $0.05 < t - T_2 < 2.5$  s). The negative drag force played a significant role in the extent of particle motion. The virtual mass force tended to act in the negative direction, but its magnitude was small.

At this point, these preliminary results are limited by several aspects. First, the velocity measurements were performed at a fixed point in space, while the video tracking data were recorded following the sediment particles: an Eulerian versus Lagrangian description. An effective method to measure simultaneously particle and fluid velocities in the same control volume is under implementation. Then, the sediment characteristics might not be representative of the fine bed materials in tidal bore affected estuaries and did not permit a study of sediment re-suspension. Earlier physical tests were performed with near-neutrally buoyant particles (Chanson and Tan, 2010) and the data exhibited some complicated suspended particle trajectories. There is a need for more realistic unsteady inflow conditions to be specified. Lastly the frame rate of the video-camera (25 fps) was relatively slow and further investigations with a faster frame rate might provide more insights into the fluid-particle interactions dynamics.

## 6. Conclusion and future work

The inception of sediment motion beneath an unsteady tidal bore flow is investigated both theoretically and physically. While the selected sediment size might not be representative of estuarine bed materials, the sediment properties and flow conditions were selected specifically to study the onset of sediment motion, with no motion during the initially steady flow conditions.

The physical results show that a large amount of gravel particles is set into bed load motion beneath the breaking bore front. The gravel particles are de-stabilized by the roller toe passage and advected upstream by bed load motion. The major result of this on-going work is the identification of the dominant contribution of the longitudinal pressure gradient force to sediment inception beneath the breaking bore. A transient recirculation next to the bed leads to a delayed drag force contribution acting in the upstream direction and adding to further transport of the particles.

Some further physical modelling is undertaken to measure simultaneously the particle and fluid velocities, to confirm these first observations and to investigate in more details the instantaneous forces acting on the sediment particles. This will be hopefully complemented with some numerical modelling.

## Acknowledgments

The authors acknowledge the technical assistance of Graham Illidge, Ahmed Ibrahim and Clive Booth. They thank Dr Pierre Lubin (University of Bordeaux) for his helpful comments and advice.

## Appendix A. Supplementary data

Supplementary data associated with this article can be found, in the online version, at doi:10.1016/j.mechrescom.2012.02.010.

## References

- Brennen, C.E., 1982. A review of added mass and fluid inertial forces. Report CR82.010, Naval Civil Eng. Lab., Department of Navy, Port Hueneme CA, USA, 50 pp.
- Chanson, H., 1999. *The Hydraulics of Open Channel Flow: An Introduction*, 1st ed. Butterworth-Heinemann, London, UK, 512 pp.

- Chanson, H., Tan, K.K., 2010. Turbulent mixing of particles under tidal bores: an experimental analysis. *Journal of Hydraulic Research IAHR* 48 (5), 641–649, doi:[10.1080/00221686.2010.512779](https://doi.org/10.1080/00221686.2010.512779).
- Chen, J., Liu, C., Zhang, C., Walker, H.J., 1990. Geomorphological development and sedimentation in Qiantang Estuary and Hangzhou Bay. *Journal of Coastal Research* 6 (3), 559–572.
- Julien, P.Y., 1995. *Erosion and Sedimentation*. Cambridge University Press, Cambridge, UK, 280 pp.
- Koch, C., Chanson, H., 2009. Turbulence measurements in positive surges and bores. *Journal of Hydraulic Research, IAHR* 47 (1), 29–40, doi:[10.3826/jhr.2009.2954](https://doi.org/10.3826/jhr.2009.2954).
- Lubin, P., Glockner, S., Chanson, H., 2010. Numerical simulation of a weak breaking tidal bore. *Mechanics Research Communications* 37 (1), 119–121, doi:[10.1016/j.mechrescom.2009.09.008](https://doi.org/10.1016/j.mechrescom.2009.09.008).
- Nino, Y., Garcia, M., 1998. Experiments on saltation of sand in water. *Journal of Hydraulic Engineering, ASCE* 124 (10), 1014–1025.
- Tessier, B., Terwindt, J.H.J., 1994. An example of soft-sediment deformations in an intertidal environment—the effect of a tidal bore. *Comptes-Rendus de l'Académie des Sciences, Série II*, vol. 319, no. 2, Part 2, pp. 217–233 (in French).